Transp Porous Med (2009) 79:407–418
DOI 10.1007/s11242-008-9330-9

Computerized Tomography Study of the Microscopic Flow Mechanism of Polymer Flooding

Jian Hou · Zhenquan Li · Sunkang Zhang · Xulong Cao · Qingjun Du · Xinwang Song

Received: 9 June 2008 / Accepted: 23 December 2008 / Published online: 10 January 2009

Abstract The microscopic flow mechanism of polymer flooding was examined using an industrial microfocus computerized tomography system. On the basis of scanned slices acquired in the process of water flooding and polymer flooding, three-dimensional visualization of oil and water distribution in different flooding conditions was achieved with a series of image processing methods, including pre-processing, interpolation, segmentation, and three-dimensional construction, which are effective techniques for both the qualitative description and the quantitative characterization of the microscopic flow mechanism. This study has confirmed the suggestion that the displacement efficiency of polymer flooding is higher than that of water flooding, and effectively revealed the microscopic mechanism of oil recovery in polymer flooding. The water/oil mobility ratio was improved after polymer flooding, which resulted in a break of the "equilibrium" flow field that was formed during water flooding and the redistribution of the regions of oil saturation. The remaining oil was flushed out as the result of the flow redirection and the viscoelastic effect of polymer flooding. Compared to water flooding, polymer flooding increased the microscopic sweep efficiency as well as the microscopic displacement efficiency, and thereby the ultimate oil recovery.

Keywords CT experiment · Water flooding · Polymer flooding · Microscopic flow

1 Introduction

Polymer flooding is one of the most effective tertiary oil recovery techniques used in China on an industrialized scale in oilfields such as Daqing and Shengli (Chang et al. 2006). Polymer

J. Hou (✉) · Q. Du
College of Petroleum Engineering, China University of Petroleum, Dongying 257061, China
e-mail: houjian@hdpu.edu.cn

Z. Li · X. Cao · X. Song
Research Institute of Geologic Science, Shengli Oilfield, Sinopec, Dongying 257015, China

S. Zhang
Research Institute of Geologic Science, Jiangsu Oilfield, Sinopec, Yangzou 225009, China

flooding increases water viscosity, increases the water/oil mobility ratio, and thereby increases oil recovery. Further development of the polymer flooding technique faces two major problems. First, most of the oil reservoirs suitable for the recovery of oil by polymer flooding have been used. The focus for improvement of polymer flooding performance will have to be moved to reservoirs with relatively harsh conditions, such as high-temperature, high-salinity reservoirs, reservoirs with edge and bottom water, and naturally fractured reservoirs. Second, polymer flooding recovers substantially more oil (6–12%) than water flooding, but only 40–50% of the geological reserves can be recovered. In other words, about half of the crude oil remains underground. Although other methods should be studied in attempts to enhance oil recovery, an in-depth study of the polymer flooding displacement mechanism, especially the micro-mechanism, has important practical significance.

Microscopic seepage experiments are attracting growing interest. Commonly used microscopic study methods include micromodeling, nuclear magnetic resonance imaging (NMR), and computerized tomography (CT). Micromodels are usually made with rocks from the reservoir, or etched glass media are used to reveal the microscopic mechanism of reservoir seepage flow through microscopic visualization of fluid flow in the model (Lago et al. 2002; Denney 2003, 2004). Currently, micromodel experiments are used widely in the study of 2D plane seepage (Dong et al. 2005; Romero-Zeron and Kantzas 2005; van Dijke et al. 2006). The spin in a magnetic field of specific atomic nuclei in rock has a characteristic resonance and relaxation behavior, which NMR uses for core analysis (Bryan et al. 2005; Dastidar et al. 2006; Toumelin et al. 2007). The working principle of CT is to use different attenuation degrees of X-rays to detect the internal structure (Hidajat et al. 2004). CT can provide an image of the rock in the absence of oil and water, can observe the distribution of oil and water in the core associated with different displacement processes, and allow study of the seepage flow properties of porous media under non-destructive, non-polluting conditions. Comparing with NMR, it will cost less money for CT scanning while ensuring study result. From the 1980s onwards, petroleum engineers began to use CT technology in core analysis to determine porosity, internal structure, and the change of fluid saturation in the course of displacement (Walsh and Withjack 1994; Schembre and Kovscek 2003; Li et al. 2005; Du et al. 2007).

For a long time, it was widely believed that polymer flooding could improve sweep efficiency and increase oil recovery, but without improvement of oil displacement efficiency. On the basis of data collected in the field and experimental results, it was thought that polymer flooding could not only improve sweep efficiency, but also improve the efficiency of oil displacement (Wang et al. 2000). The suggestion that polymer flooding can improve displacement efficiency compared with water flooding was examined in this study by the application of industrial micro-CT systems, by comparison of water flooding and polymer flooding experiments in the same core model, and by qualitative and quantitative analysis of the experimental results. The essence of the microscopic displacement mechanism in polymer flooding and the increase of oil recovery are described.

2 Materials and Methods

2.1 Analytical Instrument

This study used the ACTIS-225FFi CT/DR/RTR industrial micro-CT system (BIR Company, USA). This system is designed specifically for use in oilfields, and is different from medical CT systems. The system is equipped with two X-ray sources: a PANTAK 320 kV small focus source with strong penetration and a FeinFocus 225 kV micro focus source. This system has

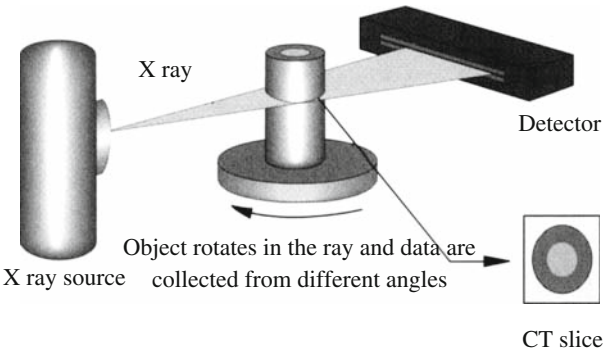

Fig. 1 Principle of CT scanning technique

very high resolution; objects with a diameter of 4.8 mm can be photographed and the spatial resolution can reach 10μm. The system has two mechanical turntables: the vertical turntable is used to scan the static characteristics of the core and for micro-imaging; the horizontal turntable is designed specifically for scanning with the core flow test device, which uses a third generation scan mode of rotating objects.

CT scanning technology is based on the Bouger–Beer law. When an X-ray penetrates an object, part of the X-ray will be absorbed or reflected. The correlation between the intensity of the X-ray after penetration I, and the incident intensity I_0, is

$$I/I_0 = \mathrm{e}^{-\mu \mathrm{h}} \tag{1}$$

where h is the thickness of the object and μ is the linear attenuation coefficient, which is related to density and effective atomic number.

In the course of CT scanning, the sample rotates at about 0.5 rpm, and I is measured from different angles for a fixed cross section, as shown in Fig. 1. This makes it possible for CT to photograph the linear attenuation coefficient in a single cross section, and a 2D cross section of the sample can be reconstructed from the strength information. The centrifugal forces in the imaging process are negligible and can be ignored.

2.2 Experimental Procedure

The same core model filled with quartz sand was used to keep the chronotaxy of the pore and throat structure between the microscopic water flooding and polymer flooding experiments. In the water flooding experiment, the core model was first vacuumized and saturated with water. The state of connate water was achieved through displacement of water with oil, and then the state of residual oil was achieved through water flooding; that is, the water cut reaches 98%. After the water flooding experiment and cleaning the core, the same model was used for the polymer flooding experiment. The procedure may be summarized as: saturate with water; saturate with oil; inject 2 PV water; inject 0.35 PV polymer; and inject water to the state of residual oil.

Taking into account the fact that the long working time of the CT scanning system will cause blurred images, and other negative effects as well as the feasibility of laboratory experiment, different displacement stages of water flooding (saturated water, saturated oil, 2 PV water flooding, residual oil after water flooding) and polymer flooding (0.35 PV polymer injection, residual oil after polymer flooding) were scanned by CT. The corresponding fluid flow was recorded in the course of the displacement experiment.

In all, 100 slicing images were scanned consecutively in the same region of the core in each course of CT scanning. The collection of each set of images took several hours, and the injection was stopped at set times to scan the images, and then the injection was started again. The total length of the scanned core was 2.5 mm, and the interval between two CT slices was 0.025 mm. A total of 600 slicing images were obtained during each set of six CT scans.

The core model was an artificial quartz sandstone model with particle sizes of 70–80#. The core permeability was 8.38μm^2, the porosity was 27.6%, the diameter of the model was 5 mm and the length was 5 cm. The density of the water solution was 1.022g/cm^3, salinity was 20.0 g/l, and the concentration of the polymer solution was 1.5 g/l. The simulated oil density was 0.88g/cm^3 and the viscosity was 72 mPa s.

3 Processing CT Images

3.1 Preprocessing

Preprocessing, including the adjustment of brightness and contrast, and image sharpening, was used because CT scanning images can suffer from dullness, blurring, and low contrast (Hou et al. 2006). Meanwhile, image truncation was done, taking into account the establishment of a 3D cubic network model. The same rectangular region in the series of CT images was chosen as the region for 3D reconstruction.

3.2 Interpolation

Since the distances between slicing images was greater than the size of the pixels of the image planes, it was necessary to generate intermediate slicing images by interpolation between the original images to achieve the requirement that vertical distances between slices after interpolation are equivalent to those of the image pixels. The simplest interpolation method is to calculate the average of adjacent slicing images to generate a group of images (Zou and Yin 2004). According to the resolution of the 2D slicing images of the core sample model and the spacing between CT scanning slice images, 331 images were obtained from the 100 CT slice scanning images of each scanning stage after interpolation. The image analysis for the interpolation images is described below.

3.3 Segmentation

Pore images can be separated from microscopic displacement images with the help of image segmentation. The traditional threshold determination method is to manually set a single threshold (Ruzyla 1986), which will often be greatly in error. Therefore, indicator Kriging, which considers the spatial distribution of pixels, was used to segment the microscopic CT images after interpolation, as shown in Fig. 2. The white region represents water. The gray region represents oil, and the oil and water are distributed in pore spaces. The black region represents rock particles.

3.4 3D Reconstruction

A group of sequential 2D slicing images was obtained by CT scanning. Information about rock particles, pore space, and fluid distribution after 2D image processing can be converted into 3D images through reconstruction, and a data field of the 3D image can be obtained,

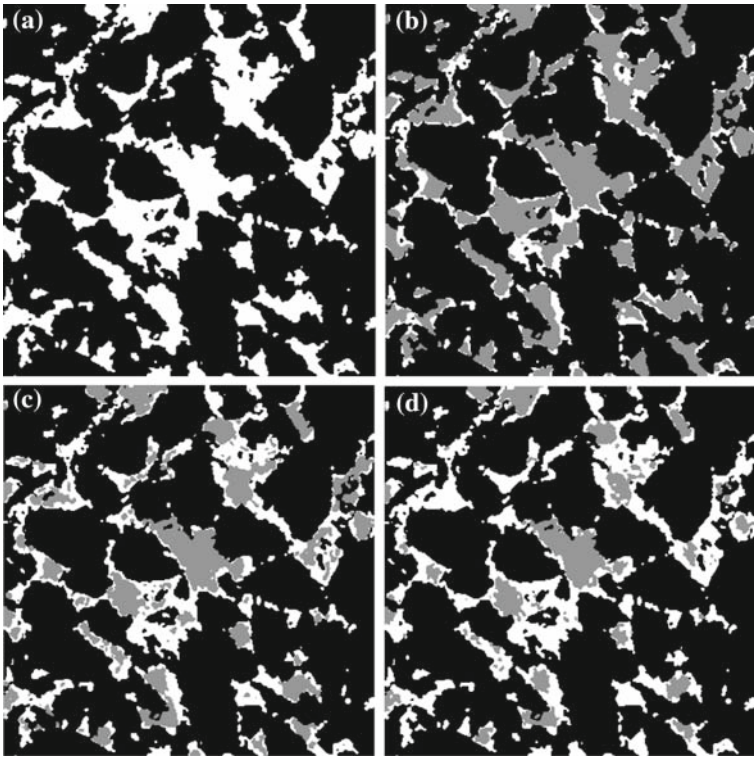

Fig. 2 Segmentation results of CT microscopic displacement images (331 × 331 pixels) in different displacement stages. **a** Saturated water, **b** saturated oil, **c** 2 PV water flooding, and **d** residual oil after water flooding

thereby achieving 3D visualization (Fig. 3). The Marching Cubes computer graphics algorithm (Lorensen and Cline 1987) was used to achieve 3D reconstruction of the CT slicing images.

3.5 Calculation of Macroscopic Parameters

Macroscopic parameters such as porosity, fluid saturation, and displacement efficiency were calculated in the course of image processing. N_P is the number of pixels corresponding to pore space, and N_T is the total number of pixels in the 3D object region. The porosity in the object region is:

$$\phi = N_P / N_T \tag{2}$$

N_o is the number of pixels corresponding to the oil remaining in the 3D object region, and the oil saturation S_o is:

$$S_o = N_o / N_P \tag{3}$$

In the process of CT scanning, if the resolution and scanning region are unchanged, the initial oil saturation is S_{oi} and oil saturation at a given displacement is S_o, then the corresponding displacement efficiency is:

$$\eta = (S_{oi} - S_o) / S_{oi} \tag{4}$$

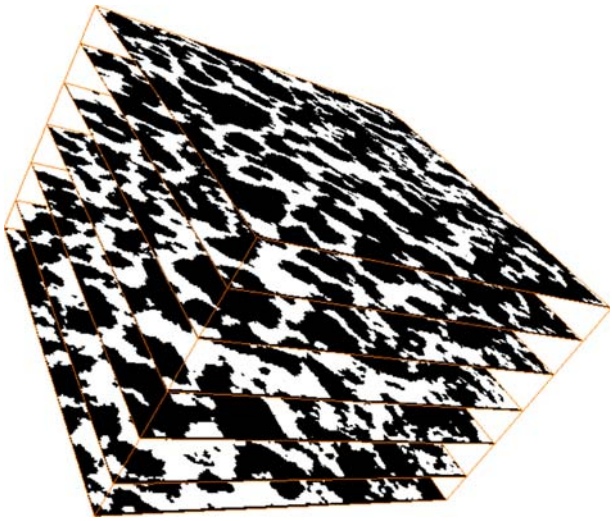

Fig. 3 3D reconstruction schematic diagram of slicing image

Table 1 Calculated results of macroscopic parameters

	CT scanning stages	Calculated oil saturation (%)	Experiment oil saturation (%)	Relative error (%)	Calculated displacement coefficient (%)	Experiment displacement coefficient (%)
Water flooding	Saturated oil	74.7	77.8	3.98	–	–
	2 PV water flooding	48.5	51.9	6.55	35.1	33.3
	Residual oil after water flooding	42.1	44.4	5.18	43.6	42.9
Polymer flooding	0.35 PV polymer injection	39.0	–	–	46.2	–
	Residual oil after polymer flooding	31.9	33.3	4.20	56	55.1

4 Results

4.1 Macroscopic Parameters

According to the image segmentation results, the calculated porosity was 27.5%. The core porosity was 27.6% according to the experiment, which is very close to the calculated value. Since the region of CT scanning is in the small-scale to micro-scale range, the variation of average oil saturation could be considered to reflect the changes of displacement efficiency. Oil saturation and the displacement efficiency were calculated according to the calculated porosity and compared with the experimental results for fluid flow, as shown in Table 1. There was a satisfactory agreement between the calculated and the experimental results.

4.2 3D Reconstruction

There is a single-phase fluid distribution in a core saturated with water, which facilitates the study of pore space distribution. The 331 CT slicing images of the saturated water core model

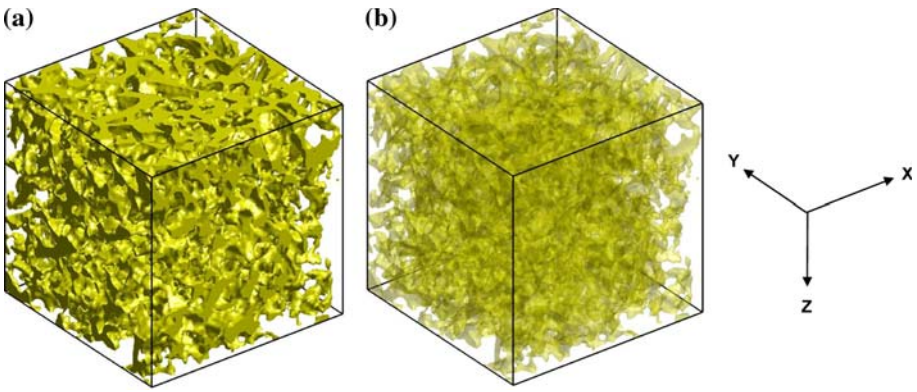

Fig. 4 3D reconstruction results of pore space images in core model (size of model: 2.45 mm × 2.45 mm × 2.45 mm). **a** Photo of pore space and **b** perspective of pore space

after interpolation were used to construct the 3D data field. The Marching Cubes algorithm was used for 3D reconstruction on the basis of segmented pore space, as shown in Fig. 4, where the yellow region represents pore space.

The 3D reconstruction was done on the basis of the 331 slices obtained by interpolation from five CT scans (saturated oil, 2 PV water flooding, residual oil after water flooding, 0.35 PV polymer injection, and residual oil after polymer flooding) of water flooding and polymer flooding. The distribution of oil and water after 2D segmentation was the reconstruction object, and the results are shown in Fig. 5. The distribution of the remaining oil is presented; red represents oil, and yellow represents pore space not saturated with oil, which is the space occupied by water.

4.3 Oil Saturation Distribution

The distribution of oil saturation after water flooding and polymer flooding of the XY, XZ, and YZ planes in different scans were calculated along the *Z* direction (i.e., displacement direction), the *X* direction, and the *Y* direction, respectively. The results are given in Fig. 6, which shows that, in the direction perpendicular to the displacement (*X* and *Y* direction), oil saturation slicing images fluctuate about the average oil saturation of different CT scans with no apparent trend, while the images change greatly along the flooding direction (*Z* direction), and display a trend; the core is placed vertically with a downward displacement. Due to the different density of oil and water, oil saturation along the direction of the CT scanning is gradually reduced in the slicing images.

In the displacement experiment, polymer flooding was shown to increase displacement efficiency by 12.2% compared to water flooding, which is consistent with the literature's conclusion (Wang et al. 2000). In order to study the mechanism underlying the increased oil recovery, the oil saturation results at different displacement periods and different time points in the *Z* direction were drawn with the same coordinate system, as shown in Fig. 7.

Displacement fluid viscosity increased after injecting 0.35 PV polymer, resulting in the loss of "equilibrium" in the water flooding system seen with the original difference of mobility between water and oil; thus, oil saturation was redistributed. Oil saturation of each slice along the displacement direction fluctuates around a constant value. In the process of polymer flooding, because of the increased mobility ratio, the oil in slices with high oil saturation

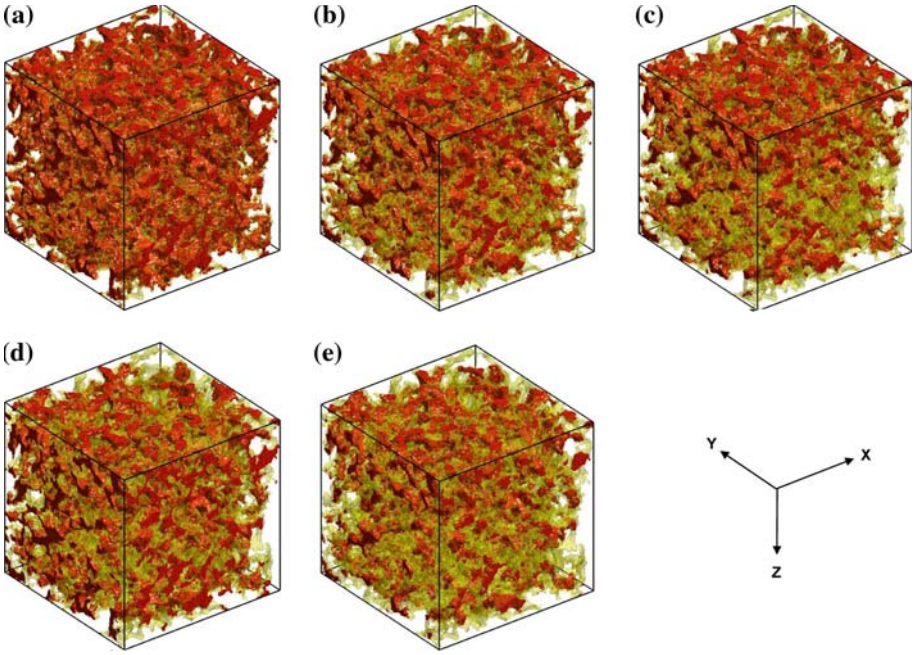

Fig. 5 3D reconstruction results of distribution of remaining oil in pore pace in different displacement stages. **a** Saturated oil, **b** 2 PV water flooding, **c** residual oil after water flooding, **d** 0.35 PV polymer injection, and **e** residual oil after polymer flooding

after water flooding is effectively displaced and flooded forward, gradually forming "oil abundance zones." The difference in oil saturation between the 0.35 PV polymer flooding stage and the 2 PV water flooding stage during the period of polymer injection is shown in Fig. 7, where positive values can be found in the figure.

During the subsequent water flooding period, the effect of the polymer diminished gradually, the mobility ratio between the subsequent injected water and the oil gradually resumed the initial state, and the distribution of oil saturation tended to return to the original oil displacement "equilibrium" state. By comparing the oil saturation at the subsequent water flooding and polymer injection periods, we see the opposite trend, i.e., the slices with a large change of oil saturation during the polymer injection period showed a relatively smaller change of oil saturation during the subsequent water flooding period, which resulted in similar oil saturation distribution at the 2 PV water flooding stage and the residual oil stage after polymer flooding.

In order to summarize, the essence of the improvement in displacement efficiency in polymer flooding lies in the fact that the polymer increases the oil/water mobility ratio, breaks the "equilibrium" system, and results in the re-distribution of oil saturation.

4.4 Microscopic Distribution of the Remaining Oil

Oil saturation is the macroscopic reflection of microscopic oil distribution, and oil saturation changes in the slicing images reflect changes of the microscopic distribution of the remaining oil. In order to observe these changes in the core model, CT scanning slices of a certain point from the XY, XZ, and YZ planes at different scanning time points were selected and drawn

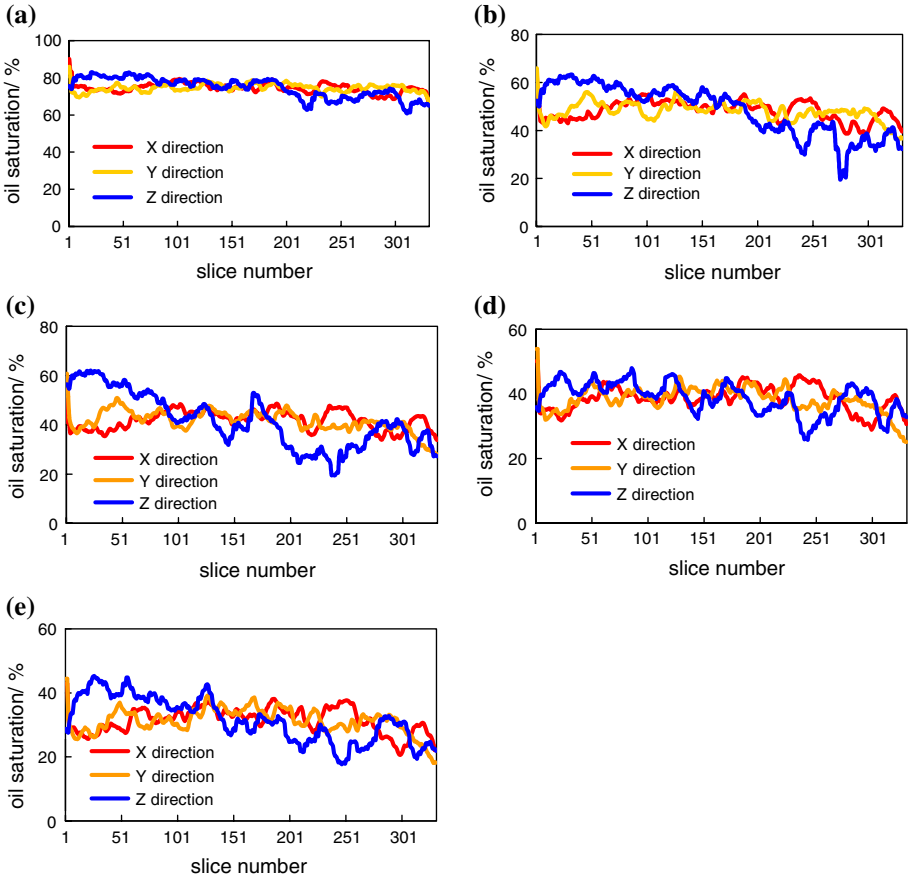

Fig. 6 Statistical results of oil saturation in different displacement stages along different direction. **a** Saturated oil, **b** 2 PV water flooding, **c** residual oil after water flooding, **d** 0.35 PV polymer injection, and **e** residual oil after polymer flooding

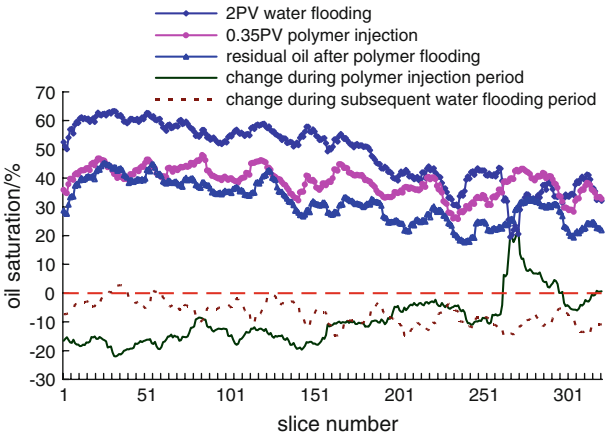

Fig. 7 Statistical results of oil saturation in different displacement along the *Z* direction

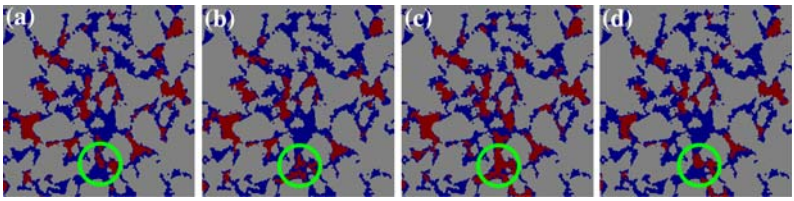

Fig. 8 Oil and water distribution of certain slice in different displacement stages along XY plane. **a** 2 PV water flooding, **b** residual oil after water flooding, **c** 0.35 PV polymer injection, and **d** residual oil after polymer flooding

as colored images with image processing, as shown in Figs. 8, 9, and 10, where red represents oil, blue represents water, and gray represents rock, and the center of the circle is the point where slice intersections are made in 3D space.

(1) By comparing the images taken during 2 PV water flooding with the residual oil state of water flooding (Figs. 8, 9, 10a, b), we can see that the pores and throats occupied by the remaining oil are basically the same, which indicates that the oil recovery in this period is produced from the pores and throats swept by the original injection of water at the 2 PV water flooding stage; in other words, because of the effects of the capillary force and displacement pressure, oil remaining in small pores and throats after water flooding often cannot be removed by further water flooding, as shown in Figs. 8, 9, and 10a.

(2) With the injection of polymer, the change of the mobility ratio of oil and water changes the waterways and flushes out the oil from the pores. Local oil abundance zones are formed in some large pores and throats, as shown in Figs. 8, 9, and 10c.

(3) Comparison of the residual oil states after water flooding and after polymer flooding (Figs. 8, 9, 10b, d) revealed an improvement of displacement efficiency by polymer flooding, which can in turn improve microscopic sweep efficiency and the microscopic displacement efficiency. The oil in pores and throats, especially in small pores and long, thin throats, which cannot be swept out by water flooding, was effectively pulled out in the process of polymer flooding due to flow redirection and the viscoelastic effect of the polymer, resulting in the improvement of microscopic sweep efficiency. Meanwhile, after polymer flooding, there was an obvious improvement of microscopic displacement efficiency in pores and throats containing a great deal of residual oil after water flooding. This is mainly because the water breakthrough effect decreased and thereby displacement became smoother after the increase of the oil/water mobility ratio. The dragging effect due to the viscoelastic nature of the polymer also had a role.

(4) In the images obtained after polymer flooding (Figs. 8, 9, 10d), the remaining oil is more dispersed due to the increasing production, and there is almost no oil connecting several pores and throats in the slices. Meanwhile, because the core is water-wet, any oil remaining is located in a central strip. However, there are still regions with abundant remaining oil in large pores due to the connecting throats. Recovering this oil will be the objective of further enhancing displacement efficiency after polymer flooding.

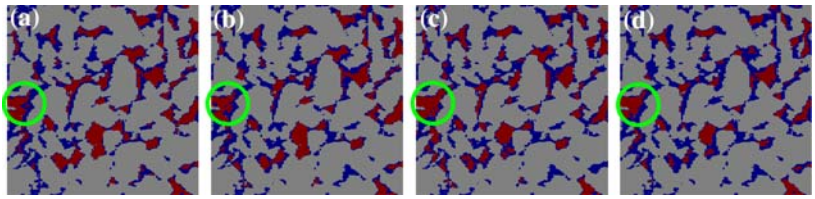

Fig. 9 Oil and water distribution of certain slice in different displacement stages along XZ plane. **a** 2 PV water flooding, **b** residual oil after water flooding, **c** 0.35 PV polymer injection, and **d** residual oil after polymer flooding

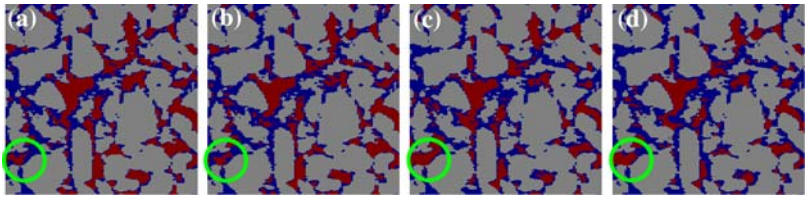

Fig. 10 Oil and water distribution of certain slice in different displacement stages along YZ plane. **a** 2 PV water flooding, **b** residual oil after water flooding, **c** 0.35 PV polymer injection, and **d** residual oil after polymer flooding

5 Conclusions

(1) Microscopic displacement experiments with polymer flooding and water flooding were done with an industrial CT system. The visualization of oil and water distribution in the core model in different displacement stages was achieved by image preprocessing, interpolation, segmentation, and 3D reconstruction, which together provide an effective method for microscopic filtration studies. The CT image processing method was verified through the calculation and comparative analysis of macroscopic seepage parameters.

(2) The results of the experiments described here show that polymer flooding can improve the ultimate displacement efficiency compared with water flooding. The essence of improving displacement efficiency in polymer flooding lies in the fact that polymer flooding can increase the oil/water mobility ratio, break the "equilibrium" system to divert waterways, and redistribute oil saturation.

(3) From the aspect of microscopic seepage, due to the combined effects of the diversion of waterways and the viscoelasticity of the polymer, the remaining oil is flushed out and removed smoothly from the pores and throats in the process of polymer flooding. Compared with water flooding, polymer flooding can improve the microscopic sweep efficiency and the microscopic displacement efficiency, and thereby the ultimate oil recovery.

Acknowledgements The writers greatly appreciate the financial support of the National Natural Science Foundation of China (Grant No. 10302021, 10772200).

References

Bryan, J., Kantzas, A., Bellehumeur, C.: Oil-viscosity predictions from low-field NMR measurements. SPE Reserv. Eval. Eng. **8**(1), 44–52 (2005)

Chang, H.L., Zhang, Z., Wang, Q., Xu, Z., Guo, Z., Sun, H., Cao, X., Qiao, Q.: Advances in polymer flooding and alkaline/surfactant/polymer processes as developed and applied in the People's Republic of China. J. Pet. Technol. **58**(2), 84–89 (2006). doi:10.2118/89175-MS

Dastidar, R., Rai, C.S., Sondergeld, C.H., Shahreyar, R.: NMR response of two clastic reservoirs: influence of depositional environment. Petrophysics **47**(3), 214–222 (2006)

Denney, D.: Investigating foamy-oil flow with a high-pressure etched-glass micromodel. J. Pet. Technol. **55**(10), 54–55 (2003)

Denney, D.: Characterization of water injection in low-permeability rock using sandstone micromodels. J. Pet. Technol. **56**(5), 71–72 (2004)

Dong, M., Foraie, J., Huang, S., Chatzis, I.: Analysis of immiscible water-alternating-gas (WAG) injection using micromodel tests. J. Can. Petrol. Technol. **44**(2), 17–24 (2005)

Du, D., Zitha, P.L.J., Uijttenhout, M.G.H.: Carbon dioxide foam rheology in porous media: a CT scan study. Soc. Pet. Eng. J. **12**(2), 245–252 (2007)

Hidajat, I., Mohanty, K.K., Flaum, M., Hirasaki, G.J.: Study of Vuggy carbonates using NMR and X-ray CT scanning. SPE Reserv. Eval. Eng. **7**(5), 365–377 (2004)

Hou, J., Zhang, S., Yuan, S.: Quantitative analysis of remaining oil in polymer flooding microscopic seepage images. J. Hydrodyn. Ser. A **21**(1), 41–45 (2006) (in Chinese)

Lago, M., Huerta, M., Gomes, R.: Visualization study during depletion experiments of Venezuelan heavy oils using glass micromodels. J. Can. Petrol. Technol. **41**(1), 41–47 (2002)

Li, G., Karpyn, Z.T., Halleck, P.M., Grader, A.S.: Numerical simulation of a CT-scanned counter-current flow experiment. Transp. Porous Media **60**(2), 225–240 (2005). doi:10.1007/s11242-004-5738-z

Lorensen, W.E., Cline, H.E.: Marching cubes: a high resolution 3D surface construction algorithm. Comput. Graph. (ACM) **21**(4), 163–169 (1987). doi:10.1145/37402.37422

Romero-Zeron, L., Kantzas, A.: Pore-scale visualization of foamed gel propagation and trapping in a pore network micromodel. J. Can. Petrol. Technol. **44**(5), 44–50 (2005)

Ruzyla, K.: Characterization of pore space by quantitative image analysis. SPE Form. Eval. **1**(4), 389–398 (1986)

Schembre, J.M., Kovscek, A.R.: A technique for measuring two-phase relative permeability in porous media via X-ray CT measurements. J. Petrol. Sci. Eng. **39**(1–2), 159–174 (2003). doi:10.1016/S0920-4105(03)00046-9

Toumelin, E., Torres-Verdin, C., Sun, B., Dunn, K.: Random-walk technique for simulating NMR measurements and 2D NMR maps of porous media with relaxing and permeable boundaries. J. Magn. Reson. **188**(1), 83–96 (2007). doi:10.1016/j.jmr.2007.05.024

van Dijke, M.I.J., Sorbie, K.S., Sohrabi, M., Danesh, A.: Simulation of WAG floods in an oil-wet micromodel using a 2-D pore-scale network model. J. Petrol. Sci. Eng. **52**(1–4), 71–86 (2006). doi:10.1016/j.petrol.2006.03.014

Walsh, M.P., Withjack, E.M.: Some remarkable observations of laboratory dispersion using computed tomography (CT). J. Can. Petrol. Technol. **33**(4), 36–44 (1994)

Wang, D., Cheng, J., Yang, Q.: Viscous-elastic polymer can increase micro-scale displacement efficiency in cores. Acta Petrol. Sin. **21**(5), 45–51 (2000) (in Chinese)

Zou, C., Yin, X.: 3-D matching interpolation based on images segmentation. Comput. Eng. Appl. **40**(24), 80–82 (2004) (in Chinese)